American Physiological Society | Journal of Neurophysiology

PUBLISHED ARTICLE
ARCHIVES
SUBSCRIPTIONS
SUBMISSIONS
CONTACT US

J Neurophysiol. 2012 May 15; 107(10): 2782–2793.
Published online 2012 Feb 22. doi: 10.1152/jn.01129.2011

PMCID: PMC3362282

Nicotinic neuromodulation in auditory cortex requires MAPK activation in thalamocortical and intracortical circuits

Irakli Intskirveli and Raju Metherate

Department of Neurobiology and Behavior and Center for Hearing Research, University of California, Irvine, California
Corresponding author.
Address for reprint requests and other correspondence: R. Metherate, Univ. of California, Irvine, 2205 McGaugh Hall, Irvine, CA 92697-4550 (e-mail: raju.metherate@uci.edu).

Received 2011 Dec 12; Accepted 2012 Feb 18.

Abstract

Go to: Go to:

Activation of nicotinic acetylcholine receptors (nAChRs) by systemic nicotine enhances sensory-cognitive function and sensory-evoked cortical responses. Although nAChRs mediate fast neurotransmission at many synapses in the nervous system, nicotinic regulation of cortical processing is neuromodulatory. To explore potential mechanisms of nicotinic neuromodulation, we examined whether intracellular signal transduction involving mitogen-activated protein kinase (MAPK) contributes to regulation of tone-evoked responses in primary auditory cortex (A1) in the mouse. Systemic nicotine enhanced characteristic frequency (CF) tone-evoked current-source density (CSD) profiles in A1, including the shortest-latency (presumed thalamocortical) current sink in layer 4 and longer-latency (presumed intracortical) sinks in layers 2–4, by increasing response amplitudes and decreasing response latencies. Microinjection of the MAPK kinase (MEK) inhibitor U0126 into the thalamus, targeting the auditory thalamocortical pathway, blocked the effect of nicotine on the initial (thalamocortical) CSD component but did not block enhancement of longer-latency (intracortical) responses. Conversely, microinjection of U0126 into supragranular layers of A1 blocked nicotine's effect on intracortical, but not thalamocortical, CSD components. Simultaneously with enhancement of CF-evoked responses, responses to spectrally distant (nonCF) stimuli were reduced, implying nicotinic "sharpening" of frequency receptive fields, an effect also blocked by MEK inhibition. Consistent with these physiological results, acoustic stimulation with nicotine produced immunolabel for activated MAPK in A1, primarily in layer 2/3 cell bodies. Immunolabel was blocked by intracortical microinjection of the nAChR antagonist dihydro-β-erythroidine, but not methyllycaconitine, implicating α4β2*, but not α7, nAChRs. Thus activation of MAPK in functionally distinct forebrain circuits—thalamocortical, local intracortical, and long-range intracortical—underlies nicotinic neuromodulation of A1.

Keywords: nicotine, acetylcholine, mouse

NICOTINE ADMINISTRATION in humans and animal models enhances sensory-cognitive function, producing, for example, enhanced processing of attended sensory stimuli (Hasselmo and Sarter 2011; Kassel 1997; Levin et al. 2006). Nicotinic enhancement of sensory-cognitive function likely involves regulation of cortical processing, and in primary auditory cortex (A1) nicotine produces apparent neuromodulatory actions that can enhance responsiveness and selectivity to sensory stimuli (Kawai et al. 2011; Liang et al. 2008). Such effects are neuromodulatory in that they alter cortical responsiveness to acoustic inputs and can endure for tens of minutes (Metherate 2011b).

Nicotinic actions that are neuromodulatory contrast with a large literature establishing the nicotinic acetylcholine receptor (nAChR) as the prototypic ionotropic neurotransmitter receptor (Albuquerque et al. 2009; Lester and Dani 1995; Miyazawa et al. 2003). The nAChR is a ligand-gated ion channel that activates rapidly and, depending on subunit composition, also can desensitize rapidly in the continued presence of agonist (Pidoplichko et al. 1997; Zhang et al. 1994). Potential mechanisms that could underlie long-lasting "modulatory" actions have been identified in diverse brain regions and include *1*) nicotinic activation of diffuse neurotransmitter systems (e.g., midbrain dopaminergic neurons) that, in turn, exert conventional neuromodulatory actions in other regions (Azam et al. 2003; Hasselmo and Sarter 2011), *2*) sustained activation by circulating nicotine of a weakly desensitizing component of the nAChR response (Lester and Dani 1995; Picciotto et al. 2008; Pidoplichko et al. 1997), or *3*) activation of intracellular signaling pathways (Chang and Berg 2001; Dajas-Bailador and Wonnacott 2004; Morley and Happe 2000). The present study explores the last possibility, the involvement of signal transduction pathways in nicotinic regulation of auditory cortex.

Studies have implicated mitogen-activated protein kinase (MAPK) in nicotinic regulation of neurons and nonneuronal tissue. Systemic nicotine increases levels of phosphorylated (activated) extracellular signal-related kinase (ERK)1/2, a member of the MAPK family, in forebrain neurons as measured by immunocytochemistry or Western blot (Brunzell et al. 2003; Steiner et al. 2007; Valjent et al. 2004). Such results are consistent with a growing body of evidence from neuronal and nonneuronal preparations that MAPK mediates some effects of nicotine (Chang and Berg 2001; Dajas-Bailador and Wonnacott 2004; Song et al. 2008). Here, we investigate the role of MAPK in nicotinic regulation of tone-evoked responses in mouse A1. We find that MAPK activation in three functionally distinct thalamocortical and intracortical circuits underlies enhancement of responses to characteristic frequency (CF) stimuli and suppression of responses to spectrally distant (nonCF) stimuli. Activation of MAPK in A1 requires nAChRs that also are located in A1. These results indicate that MAPK mediates nicotinic neuromodulation of A1 to enhance the processing of acoustic information within more narrowly focused receptive fields. The results are incompatible with alternative explanations (above) involving diffuse neurotransmitter systems or sustained action of circulating nicotine.

MATERIALS AND METHODS

Go to: Go to:

Animals. Adult (~90 day old) male FVB mice were used for all procedures in accordance with the National Institutes of Health *Guide for the Care and Use of Laboratory Animals* and as approved by the University of California, Irvine Institutional Animal Care and Use Committee (IACUC). Mice were anesthetized with urethane (0.7 g/kg ip; Sigma) and xylazine (13 mg/kg ip; Phoenix Pharmaceutics), placed in a sound-attenuating chamber (AC-3; IAC) and maintained at 37°C. Anesthesia was supplemented as necessary with urethane (0.13 g/kg) and xylazine (13 mg/kg) via an intraperitoneal catheter to avoid movement of mice. The head was secured in a stereotaxic frame (model 923; Kopf Instruments) with blunt earbars. After a midline incision, the skull was cleared and secured to a custom

head holder. A craniotomy was performed over the right auditory cortex, and the exposed brain was kept moist with warmed saline. In some cases a second craniotomy was made to permit microinjections into the thalamus. After the craniotomy, the blunt earbars were removed to permit acoustic stimulation.

Electrophysiology and acoustic stimulation. Tone-evoked local field potentials (LFPs) were recorded with a glass micropipette filled with 1 M NaCl (~1 MΩ at 1 kHz) for mapping A1 or a 16-channel silicon multiprobe (~2–3 MΩ at 1 kHz for each 177-μm^2 recording site, 100-μm separation between recording sites; NeuroNexus Technologies) for CSDs and were filtered and amplified (1 Hz to 10 kHz, AI-401 or AI-405, CyberAmp 380; Axon Instruments), digitized, and stored on a computer (Apple Macintosh running AxoGraph software). Acoustic stimuli were digitally synthesized and controlled with MALab (Kaiser Instruments) and a computer (Macintosh) and delivered through an open-field speaker (ES-1 or FF-1 with ED-1 driver; Tucker-Davis Technologies) positioned ~3 cm in front of the left ear. For calibration [sound pressure level (SPL), in dB re: 20 μPa] a microphone (model 4939 and Nexus amplifier; Brüel and Kjaer) was positioned in place of the animal at the tip of the left earbar. Tones were 100 ms in duration with 5-ms linear rise and fall ramps and ranges of 1–40 kHz and −10 dB to 70 dB SPL. During data collection, stimuli were delivered at a rate of 1/s in sets of 25 trials.

Determination of A1 recording site. To find a recording site in A1, we modified our method previously described for rat (Kaur et al. 2005). Initially, we recorded tone-evoked responses from multiple sites ~250 μm apart along the anterior-posterior axis in auditory cortex, using a glass micropipette. Based on responses to a standard set of tones (1–40 kHz in 2.5-kHz steps, −10 dB to 70 dB SPL in 5-dB steps), we determined CF (frequency with the lowest threshold) for each recording site. Initial maps of CF were determined from LFP recordings at the cortical surface, with subsequent confirmation at a few sites by multiunit recordings in layer 4 (~400-μm depth). CF maps were constructed to confirm the tonotopy expected for A1, including a reversal of tonotopy at the border with the anterior auditory field (Stiebler et al. 1997). We then chose a site within A1 having a CF of 10–20 kHz and mapped along the dorsoventral axis of the presumed isofrequency region to find the site with the shortest-latency, largest-amplitude surface LFP. This site was used for all subsequent procedures. We inserted a 16-channel multiprobe perpendicular to the pial surface to record LFPs throughout the cortical depth and redetermined more precisely CF (1-kHz steps) and threshold (5-dB steps) based on the initial slope and onset latency of LFPs recorded 300–400 μm below the surface. Tone-evoked LFPs were considered threshold responses when their amplitude exceeded 3 standard deviations from the baseline value determined over the 100 ms preceding the tone.

Drug application. Nicotine hydrogen tartrate (Sigma) was dissolved in saline and adjusted to pH 7.0 before systemic injection. The nicotine dose is reported as free base (1 mg/kg nicotine hydrogen tartrate = 0.35 mg/kg free base) and was delivered subcutaneously. The MAPK-ERK kinase (MEK) inhibitor U0126 and its inactive analog U0124 (Calbiochem) were stored at −20°C as stock solutions in DMSO. Immediately before injection the stock was diluted in artificial cerebrospinal fluid (ACSF; in mM: 125 NaCl, 2.5 KCl, 25 $NaHCO_3$, 1.25 KH_2PO_4, 1.2 $MgSO_4$, 2.0 $CaCl_2$, 10 dextrose) to 20 μM (2% final DMSO concentration). The injected solution also contained 2% tetramethylrhodamine dextran (10 kDa; Invitrogen) or fluorescein dextran (10 kDa; Invitrogen) to mark injection sites. For thalamic and cortical microinjections we used a 0.5-μl Hamilton syringe fitted with a glass pipette (~20-μm tip). During injections an ~100 nl (thalamus) or ~50 nl (cortex) volume was delivered slowly over 5 min, and the injector was removed from the brain after an additional 10 min (after which tone-evoked responses were collected for ~30 min before administration of nicotine, e.g., Fig. 3). Thalamic injections targeted the superior thalamic radiation (STR), which contains the initial ~1 mm of the

auditory thalamocortical pathway before it emerges from the thalamus proper (Cruikshank et al. 2002). Stereotaxic coordinates were (mm from bregma) AP 1.5–1.6, ML 2.2–2.3, and DV −2.8. Cortical injections targeted the supragranular cortex close to the multiprobe. To locate injection sites, after each experiment the animal was perfused with 4% paraformaldehyde and the brain was sectioned in the thalamocortical (thalamic injections) or coronal (cortical injections) plane. Sections (~50-μm thick) were mounted on a glass slide and imaged with a digital camera (AxioCam and Axioskop microscope; Zeiss) and software (OpenLab; Improvision). The brightest (center) region of fluorescence was designated as the injection site.

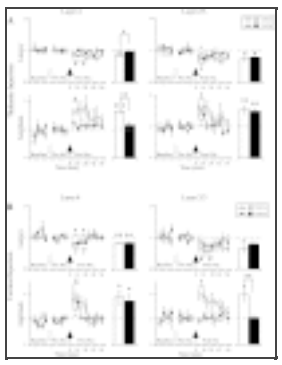

Fig. 3.
Time course and peak magnitude of systemic nicotine's effects on CF-evoked current sinks in layers 4 and 2/3 after thalamic (*A*) or intracortical (*B*) microinjection of control drug (U0124) or MEK inhibitor (U0126). Measurements reflect thalamocortical **...**

Physiology data analysis. Each tone-evoked response is the average response to 25 stimuli, and responses to CF and nonCF stimuli at threshold and two higher intensities were determined at regular intervals before and after drug administration. CSD profiles were constructed off-line as described previously (Kaur et al. 2005; Kawai et al. 2007). One-dimensional CSD profiles are the second spatial derivative of the LFP laminar profile (Muller-Preuss and Mitzdorf 1984); conventionally, a current sink implies the location, timing, and magnitude of underlying synaptic excitation. The onset of a CSD trace was defined as the time at which the response crossed a threshold 2 standard deviations above baseline. The middle-layer CSD trace with shortest onset latency (typically 200–400 μm depth) was designated the initial sink and its initial amplitude considered a reflection of monosynaptic thalamocortical input (note, however, that this middle-layer sink often is preceded by a deeper sink in layer 5–6; see Fig. 1). Current sink magnitudes were measured in two ways: The initial sink's initial amplitude was measured 5 ms after onset, and for all sinks we measured peak amplitude over the first 100 ms (i.e., up to tone offset). To obtain group CSD profiles (e.g., Fig. 2), individual prenicotine profiles were normalized to the largest-amplitude current sink, aligned so that the initial (thalamocortical) sink was placed at the same depth (designated mid-layer 4 in figures), and averaged across animals.

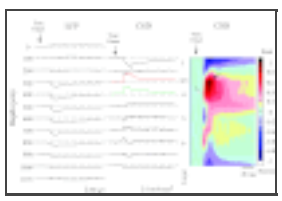

Fig. 1.
Laminar profile of characteristic frequency (CF) tone-evoked responses in A1. *Left*: representative example of local field potentials (LFPs) recorded with a 16-channel silicon multiprobe (12 channels shown, with the trace from the recording site visible **...**

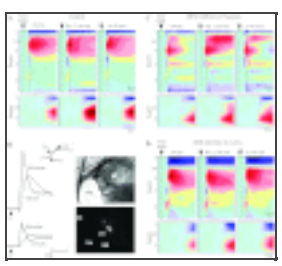

Fig. 2.
Effects of systemic nicotine on group CSD profiles in A1 for control animals (*A*) and after thalamic (*C*) or intracortical (*D*) microinjection of MEK inhibitor. *A*: nicotine enhanced CSD profiles evoked by CF stimuli (70 dB, $n = 7$) after control injections **...**

Laminar analysis. To relate CSD profiles to cortical laminae, we measured cortical thickness in the 20-kHz region of A1 in a separate group of adult animals and subdivided the cortex into layers per Anderson et al. (2009). A pipette containing fluorescent tracer (as above) was lowered into the 20-kHz region to mark the site. After removal of the pipette, the animal was killed and the brain was sectioned without tissue fixation with a vibrating tissue slicer (Leica). Then, in 200-μm-thick coronal sections, we measured cortical width at the injection site and nearby sites (see RESULTS).

Statistical analyses. All mean data are reported ±SE. Statistical comparisons were performed with Microsoft Excel or JMP. Tests of independent means were Student's *t*-test or factorial ANOVA ($\alpha = 0.05$). Tests of related means (e.g., time course data; Fig. 3) were multivariate analysis of variance (MANOVA) followed by post hoc paired *t*-tests (2-tailed) with Bonferroni correction. To determine drug effects, we first examined response data within each of two ~30-min time periods—predrug (baseline) and prenicotine (but after injection of U0124 or U0126)—and confirmed response stability by using multiple paired *t*-tests to show that the four response measures within each 30-min period did not differ. Recordings with unstable responses were not analyzed further. For stable responses, baseline and prenicotine data were grouped within each time period and compared to each other (paired *t*-test); prenicotine responses were compared to postnicotine responses (grouped into 14-min bins) with MANOVAs followed by appropriate post hoc tests with correction.

Immunolabeling. A separate group of adult male mice were anesthetized and prepared surgically as described above, except that two craniotomies were performed to expose auditory cortex in both hemispheres and the speaker was placed directly in front of the animal, 3 cm from its nose. Using stereotaxic coordinates (2.75 mm posterior and 4.25 mm lateral to bregma), we placed a glass microelectrode on the cortical surface or in layer 4 (400-μm depth) and mapped (250-μm spacing) the cortical response to click stimuli in each hemisphere. We selected the site with the shortest onset latency and a robust response, presumably within A1, for microinjection of drugs or control solution (ACSF) prior to acoustic stimulation and subsequent immunohistochemistry. For microinjection we used a glass micropipette with a ~20-μm tip fitted on a 0.5-μl Hamilton syringe. Microinjections (50-nl volume delivered over 5 min) were made at a depth of ~200 μm and consisted of ACSF or the nAChR antagonists dihydro-β-erythroidine (DHβE, 1 μM) or methyllycaconitine (MLA, 10 nM) to block α4β2* nAChRs (asterisk indicates presence of additional subunits) or α7 nAChRs, respectively, with 2% fluorescein dextran (10 kDa, Invitrogen) for post hoc visualization of the injection site. Immediately after microinjection, we presented white noise bursts repeatedly for 15 min (50 dB, 100-ms duration, 5-ms rise/fall ramps, 0.5 stimuli/s) followed by systemic nicotine as before. After another 5 min of white noise stimulation, the animal was removed from the acoustic chamber for transcardial perfusion.

Animals were deeply anesthetized and perfused transcardially with ice-cold phosphate-buffered saline (PBS), followed by 4% paraformaldehyde in PBS. Brains were removed and placed in the same fixative overnight and then rinsed with PBS and sectioned along the horizontal plane (40-μm sections; VF-200 microtome, Precisionary Instruments). Sections were rinsed in PBS and incubated for 90 min in a blocking solution of 5% donkey serum and 0.3% Triton X-100 in PBS at room temperature. Sections were then placed in a solution containing the primary antibody against phosphorylated ERK [phospho-p44/42 MAPK (Erk1/2) (Thr202/Tyr204) MAPK antibody, 1:400, rabbit monoclonal antibody; Cell Signaling Technology no. 4370] (Abdala-Valencia et al. 2011; Faber et al. 2011) in blocking solution (5% donkey serum and 0.3% Triton X-100 in PBS) at 40°C for 24 h. After the sections were washed for 10 min three times in PBS, sections were incubated with secondary antibody

(1:250 Alexa Fluor 594 donkey anti-rabbit IgG; Invitrogen, Molecular Probes) in blocking solution in the dark for 120 min at room temperature. Sections were then washed for 10 min three times in PBS and then mounted on slides with Glycergel mounting medium (Dako).

Cell counting. We used a microscope (Zeiss Axioskop) equipped with a digital camera (Zeiss Axiocam) and a fluorescent light source (X-Cite; 120 Q Series, EXFO Photonic Solution). Imaging software (Zeiss AxoVision) was used to store images in florescence and normal light and at different magnifications. After the injection site was identified (fluorescent tracer), the distribution of immunolabeled cells was determined. On each horizontal slice, the cortical region of interest was divided into four 250-μm-wide bins centered on the injection site (2 anterior and 2 posterior to the center of the injection site); however, labeled cell counts did not differ by bin, and data were combined. Each bin spanned all cortical layers and itself was subdivided into five 100-μm-thick rectangles spanning the superficial half of cortex (approximately layers 1–4) and a single rectangle for the lower cortex (~layers 5–6). Using imaging software (NIH ImageJ), we measured the size and brightness of each labeled cell and counted cells as immunopositive if the brightness exceeded background by 2 standard deviations.

RESULTS

Go to: Go to:

We begin with a description of tone-evoked CSD profiles in mouse A1 and their regulation by systemic nicotine. We then show the effects of microinjecting into the thalamus or cortex the drug U0126, which selectively blocks activation of the MAPK family member ERK1/2 by inhibiting MEK, the immediately upstream kinase required for activation of ERK1/2. Thalamic injections targeted the initial portion of the auditory thalamocortical pathway, whereas cortical injections targeted supragranular layers of A1. All injection sites were confirmed (with fluorescent dye) to be in the targeted regions, but since drugs likely spread beyond the injection sites we distinguish only between cortex and thalamus when inferring locus of action. Finally, using immunolabeling techniques, we examined the distribution of cortical cells with phosphorylated (activated) MAPK and determined whether immunolabeling depended on nAChRs that also were located within A1.

Tone-evoked CSD profiles in mouse A1. After mapping to determine the location of A1 (see MATERIALS AND METHODS), we selected a recording site with a CF of ~20 kHz in order to examine responses to both CF and a second stimulus frequency ~2 octaves lower (referred to as "nonCF"). We inserted a 16-channel multiprobe electrode orthogonal to the cortical surface to record LFPs in all cortical layers simultaneously (100-μm separation between recording sites, with the first site visible at the cortical surface). At regular (~7 min) intervals before and after administration of nicotine and other drugs, tone-evoked LFPs were elicited in response to CF and nonCF stimuli at intensities ranging from below threshold to 70 dB SPL. CSD profiles were derived off-line. Results below are for stimulation at 70 dB SPL, except for an explicit comparison that confirms similar effects at different intensities (see Fig. 4).

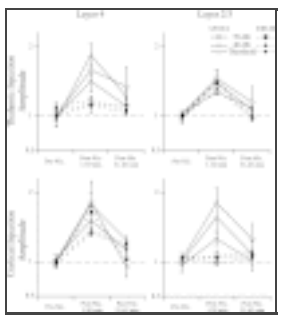

Fig. 4.
Effects of nicotine and MEK inhibition are similar at all stimulus intensities tested. Graphs show effects of nicotine on current sinks in layer 4 (initial amplitude) and layer 2/3 (peak amplitude) evoked by CF stimuli at 3 intensities: acoustic threshold ...

To relate CSD profiles to cortical layers, in five animals we measured cortical thickness within the 20-kHz CF region of A1 and subdivided the cortex into layers per the quantitative description of Anderson et al. (2009) (see MATERIALS AND METHODS). Fluorescent tracer was injected intracortically into a 20-kHz site, and the brain was removed and sectioned without fixation. Cortical thickness at the injection site averaged 1,061 ± 11.8 μm (n = 5), and similar thickness was found at sites 200 μm anterior (1,051 ± 15.3 μm) and 200 μm posterior (1,024 ± 13.2 μm; paired t-tests, all $P > 0.05$) to the injection site. Thus cortical thickness at all three sites averaged 1,045 μm, and this value was used for CSD analysis. A fourth site 400 μm anterior to the injection site—and outside A1 since it was anterior to the physiologically mapped reversal of CF between A1 and the anterior auditory field—had a thicker cortex than each site within A1 (mean 1,163 ± 13.2 μm; all $P < 0.001$). To assign recording depths to cortical layers, we used the following laminar proportions (Anderson et al. 2009): layers 1, 2, 3, and 4 occupied equal widths within the upper 50% of the cortex, and layers 5 and 6 were equally spaced within the lower 50%. These laminar proportions are consistent with our own Nissl material, which, however, was not used to estimate cortical width given the ~10% shrinkage due to fixation (width at 20-kHz injection site in fixed tissue 899 ± 16.8 μm; n = 3). Thus the cortical width of 1,045 μm at the recording site is spanned by the first 11 recording sites on the 16-channel multiprobe, and CSD profiles illustrated here span the full cortical depth.

A sample CSD profile elicited by CF stimuli is shown in Fig. 1 to illustrate the main response features. CF stimuli typically elicited one or two major current sinks (putative sites of excitatory synaptic activity) in the middle and upper layers. The initial portion (first few milliseconds) of the shortest-latency, middle-layer current sink presumably reflects thalamocortical input (at 400-μm depth, or upper layer 4; Fig. 1) (Happel et al. 2010; Kaur et al. 2004, 2005). This initial current sink peaked within ~20 ms either within the same layer (layer 4) or in a more superficial layer (200- to 300-μm depth, layer 2 or 3; Fig. 1). A shift in the location of the main sink from layer 4 to layer 2/3 over time was seen in most cases (65%, 17/26 animals). In fewer cases (35%, 9/26 mice), the peak of the main current sink remained in the input layer. Longer-latency current sinks that could endure 100 ms or more likely reflect substantial intracortical activity and were common throughout the middle and upper layers. Other common response features include current sources above and below the current sinks and, in most animals, a small but clear current sink in deeper layers (at 800-μm depth in Fig. 1) that preceded the layer 4 initial sink. Apart from this brief response, in most animals infragranular activity was weak, and tone-evoked activity typically was restricted primarily to input and supragranular layers.

Because of the similarity of CF-evoked CSD profiles across animals, we constructed group profiles (Fig. 2*A*). Individual CSD profiles were normalized to the largest-amplitude current sink in the prenicotine condition and aligned across animals by assigning the shortest-latency middle-layer current sink to the same position (designated mid-layer 4 in Fig. 2*A*). The normalized profiles were then averaged across animals. Depth in cortex was assigned to layers by using information on the relative thickness of layers (above), and layers 2 and 3 were grouped by convention and because the main sink could be found in either. Many of the same features seen in individual examples (Fig. 1) are seen in the group average, including a main (largest amplitude) sink centered either in layer 4 or layer 2/3, long-lasting intracortical sinks in layers 2–4, and little or no activity in layers 5–6 except for a weak, brief response preceding the layer 4 onset. Because variability in the laminar location of the main sink for individual animals within each group, the main sink in group profiles could be found either in layer 4 (e.g., Fig. 2*D*) or layer 2/3 (e.g., Fig. 2*A*).

Nicotinic modulation of CF-evoked CSD profiles. In preliminary experiments, systemic nicotine was

administered over a range of doses (0.7–2.1 mg/kg free base sc) to establish a low but effective dose for enhancing tone-evoked responses. The effects of nicotine were determined on the initial slope and peak amplitude of CF-evoked LFPs recorded in layer 4 with a micropipette electrode. Nicotine doses of 0.7–1.4 mg/kg are above threshold for enhancing responses in rat A1 (Liang et al. 2006) but were less effective in mouse [comparison of post- vs. prenicotine measures, paired *t*-test, $n = 7$; slope 0.97 ± 0.03 of baseline ($P = 0.6$); amplitude 0.97 ± 0.01 of baseline ($P = 0.8$)]. A higher dose of 2.1 mg/kg was more consistently effective, increasing slope to 1.64 ± 0.13 of baseline ($P = 0.01$, $n = 3$) and amplitude to 2.32 ± 0.48 of baseline ($P = 0.02$). This dose was considered reliably effective and used for all subsequent experiments.

The effect of systemic nicotine on CF-evoked CSD profiles can be seen in control experiments during which the inactive drug U0124 was injected into the thalamus or cortex. The group CSD profile is shown in Fig. 2*A* (thalamic control injection, $n = 7$; lower panels show first 20 ms after tone onset), and example CSD traces are in Fig. 2*B*. Systemic nicotine enhanced tone-evoked responses, most prominently in layers 2–4 (Fig. 2*A*). In particular, nicotine reduced the latency and increased the amplitude of the initial current sink in layer 4 and the main current sink in layer 2/3 (Fig. 2*B*). Nicotine also enhanced longer-latency sinks, but because of their variable laminar location and timing, group effects are less obvious.

These effects are consistent with previous reports of nicotinic enhancement of sensory-evoked cortical responses in LFP single unit and multiunit recordings (Harkrider and Champlin 2001; Liang et al. 2006; Oldford and Castro-Alamancos 2003; Parkinson et al. 1988). Unlike previous reports, however, the present study explicitly identifies two potential loci of nicotinic action. First, nicotinic enhancement of thalamocortical input implies a precortical locus consistent with, for example, recent evidence that nAChRs regulate excitability of auditory thalamocortical axons (Kawai et al. 2007). Second, enhancement of intracortical current sinks suggests either *1*) an intracortical locus of action or *2*) intracortical propagation of enhanced thalamocortical input. Thus the neuromodulatory effects of systemic nicotine could result from actions in the thalamocortical pathway (or any preceding auditory relay) and, possibly, intracortical circuits. To test for MAPK-mediated modulation at these loci, we injected the MEK inhibitor U0126 into either the thalamocortical pathway or supragranular A1 and then tested for effects of systemic nicotine.

Effects of thalamic or cortical microinjection of MEK inhibitor on nicotinic modulation of CSD profiles.

The MEK inhibitor U0126 (20 μM; 100 nl in thalamus or 50 nl in cortex) was microinjected 30 min prior to systemic nicotine, since such pretreatment (dose and duration) is known to selectively block MAPK activation (phosphorylation of ERK1/2) in a wide variety of tissues including rodent forebrain (Favata et al. 1998; Roberson et al. 1999; Shobe et al. 2009; Steiner et al. 2007; Welsby et al. 2009). Thalamic injections targeted the initial ~1-mm segment of the auditory thalamocortical pathway (STR); all fluorescently labeled injection sites were centered in, or largely overlapped, portions of STR. Cortical injections were centered in supragranular layers adjacent to the CSD multiprobe. Injection sites were confirmed after each experiment by visualizing the fluorescent dye injected along with drugs (Fig. 2*B*, *right*, shows a thalamic injection in STR).

Thalamic injection of MEK inhibitor preferentially reduced the effects of systemic nicotine on the tone-evoked thalamocortical current sink (Fig. 2*C*). The group CSD profile shows that nicotine clearly enhanced tone-evoked activity in supragranular layers but had lesser effects on the earliest response in layer 4 (Fig. 2*C*; lower panels show initial response in layer 4). In contrast, cortical injection of MEK

inhibitor largely blocked nicotinic enhancement of supragranular current sinks (Fig. 2*D*) without blocking the shift to shorter latencies and larger amplitudes for the initial layer 4 current sink (lower panels in Fig. 2*D*). The differential effects of thalamic versus cortical MEK inhibition imply that MAPK in two distinct loci contributes to nicotinic modulation.

To quantify these effects we focused on the major response features, as shown in Fig. 2*B*. To assess thalamocortical input we focused on the initial portion of the layer 4 current sink, measuring its onset latency and amplitude 5 ms after onset (Fig. 2*B*, *left*, *bottom* and *inset*). Then, to assess intracortical activity we measured the peak latency and peak amplitude of the current sink in layer 2/3 (Fig. 2*B*, *left*, *top*). We also measured the peak layer 4 sink (latency and amplitude), an intermediate measure that likely reflects both thalamocortical and intracortical processing. In control animals, nicotine decreased latencies and increased amplitudes for the layer 4 and layer 2/3 current sinks (Fig. 2*B*), as seen in group CSD profiles and summarized in Table 1.

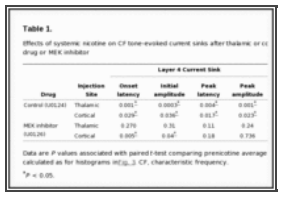

Table 1.

Effects of systemic nicotine on CF tone-evoked current sinks after thalamic or cortical injections of control drug or MEK inhibitor

Group data in Fig. 3 show the magnitude and time course of drug effects on thalamocortical input (layer 4 sink, onset latency and amplitude at 5 ms; Fig. 3, *A* and *B*, *left*) and intracortical activity (layer 2/3 sink, peak latency and amplitude; Fig. 3, *A* and *B*, *right*). Histograms in Fig. 3 and data in Table 1 summarize peak effects of nicotine over 15–30 min (or 30-min average, if no effect of nicotine). Figure 3*A*, *left*, shows the effects of thalamic drug injections. Prior to systemic nicotine, response measures were not affected by thalamic injection of the control drug, U0124 (delivered over 5 min followed by 10-min rest; all responses normalized to prenicotine values). In controls, systemic nicotine reduced latencies and enhanced amplitudes for the initial layer 4 sink (onset latency and amplitude at 5 ms; Fig. 3*A*, *left*), the peak layer 2/3 sink (peak latency and peak amplitude; Fig. 3*A*, *right*), and the peak sink in layer 4 (not shown; Table 1) [all comparisons MANOVAs, postnicotine data grouped into 14-min bins and *P* values indicate outcome of post hoc tests with Bonferroni correction, see MATERIALS AND METHODS, $n = 7$; layer 4 onset latency: $F(4,24) = 5.26$, $P = 0.0035$; layer 4 peak latency: $F(4,24) = 3.98$, $P = 0.0128$; layer 2/3 peak latency: $F(4,24) = 3.58$, $P = 0.019$; layer 4 initial amplitude: $F(4,24) = 2.79$, $P = 0.04$; layer 4 peak amplitude: $F(4,24) = 3.88$, $P = 0.014$; layer 2/3 peak amplitude: $F(4,24) = 2.78$, $P = 0.04$]. The effects of nicotine lasted ~14–28 min. Statistically significant postnicotine time points were averaged to obtain peak values shown in histograms and compared to prenicotine values (Fig. 3*A*; Table 1 lists outcome of pre- vs. postnicotine paired *t*-tests, $n = 7$). Thus nicotine increased amplitudes and decreased latencies of tone-evoked current sinks attributed to both thalamocortical and intracortical processing.

Microinjection into the thalamus of the MEK inhibitor U0126 differentially affected nicotinic regulation of thalamocortical versus intracortical responses. In the presence of thalamic MEK inhibition, systemic nicotine did not affect the onset latency or initial amplitude of the layer 4 current sink [Fig. 3*A*, *left*; MANOVAs, $n = 5$ or 6; latency: $F(4,20) = 0.753$, $P = 0.567$; amplitude: $F(4,20) = 0.74$, $P = 0.57$]. However, nicotine still reduced the peak latency and increased the peak amplitude of the layer 2/3 current sink [Fig. 3*A*, *right*; latency: $F(4,16) = 3.006$, $P = 0.05$; amplitude: $F(4,16) = 5.96$, $P = 0.003$]. The inhibitor also blocked nicotine's effect on the layer 4 sink peak latency and amplitude [$n = 6$, not shown, Table 1; latency: $F(4,20) = 1.87$, $P = 0.155$; amplitude: $F(4,20) = 0.377$, $P = 0.82$]. The effects of thalamic MEK inhibitor are summarized in the histograms and Table 1 ($n = 5$ or 6). Peak

effects of nicotine (histograms) also were compared between drug conditions and significant differences indicated in Fig. 3*A* (between-bar comparisons, ANOVA). Thus inhibition of MAPK activation in the thalamus blocked nicotine's effect on the CF-evoked layer 4 current sink but not its effect on the layer 2/3 current sink.

Nicotine's effects after intracortical injection of drugs are shown in Fig. 3*B*. For control injections (U0124), effects of nicotine closely resembled those described above for thalamic controls, i.e., reduced current sink latencies and increased amplitudes [Fig. 3*B*; MANOVAs, $n = 6$; layer 4 onset latency: $F(4,20) = 3.65$, $P = 0.02$; layer 4 peak latency: $F(4,20) = 2.45$, $P = 0.02$; layer 2/3 peak latency: $F(4,20) = 6.013$, $P = 0.002$; layer 4 initial amplitude: $F(4,20) = 10.14$, $P = 0.0001$; layer 4 peak amplitude: $F(4,20) = 5.79$, $P = 0.003$; layer 2/3 peak amplitude: $F(4,20) = 3.52$, $P = 0.02$]. Peak nicotine effects are summarized in the histograms and Table 1 (pre- vs. postnicotine, paired *t*-tests, $n = 6$).

In contrast to the effects of thalamic MEK inhibition, however, intracortical MEK inhibition blocked nicotine's effect on the intracortical (layer 2/3) sink's peak latency and amplitude but did not prevent the decreased onset latency and increased initial amplitude for the layer 4 sink [Fig. 3*B*; MANOVAs, $n = 6$; layer 4 onset latency: $F(4,20) = 3.031$, $P = 0.04$; layer 4 peak latency: $F(4,20) = 1.133$, $P = 0.37$; layer 2/3 peak latency: $F(4,20) = 1.106$, $P = 0.38$; layer 4 initial amplitude: $F(4,20) = 4.15$, $P = 0.01$; layer 4 peak amplitude: $F(4,20) = 0.9$, $P = 0.48$; layer 2/3 peak amplitude: $F(4,20) = 0.08$, $P = 0.98$]. The effects of cortical MEK inhibition are summarized in the histograms and Table 1 (pre- vs. postnicotine paired *t*-tests, $n = 6$). Peak effects of nicotine (histograms) also were compared between drug conditions and significant differences indicated in Fig. 3*B* (between-bar comparison, ANOVA). Thus inhibition of MAPK activation in the cortex reduced nicotine's effect on the CF-evoked layer 2/3 current sink but not its effect on the initial layer 4 current sink, confirming the contrasting effects of thalamic versus cortical MEK inhibition.

Note that prior to nicotine administration, injection of MEK inhibitor into the thalamus (Fig. 3*A*) or cortex (Fig. 3*B*) did not by itself affect amplitude or latency measures for any current sink (Fig. 3, paired *t*-tests comparing average baseline vs. average prenicotine responses, *P* values > 0.05), indicating that blockade of thalamic or cortical MAPK activation per se did not affect tone-evoked responses.

Comparison of results across stimulus intensity. Although the results presented above are for acoustic stimulation at 70 dB SPL, similar results were observed for CF stimuli at all intensities tested. Figure 4 summarizes the effects of nicotine on responses to CF stimuli at threshold intensity (12.5 ± 0.84 dB SPL, $n = 26$) and two higher intensities (40 dB, 70 dB), separately for the initial layer 4 current sink (Fig. 4, *left*), and the peak layer 2/3 sink (Fig. 4, *right*). After control injections of U0124 into the thalamus (Fig. 4, *top*) or cortex (Fig. 4, *bottom*), nicotine enhanced all response amplitudes at each intensity tested (Fig. 4; paired *t*-tests, *P* values < 0.05; $n = 6$ or 7 at each intensity for thalamic injections; $n = 6$ for cortical injections). Injection into the thalamus of the MEK inhibitor blocked nicotine's effect in layer 4 (Fig. 4, *top*; paired *t*-tests, $P > 0.05$, $n = 6$ at each intensity), but not in layer 2/3 ($P < 0.05$), similarly at each intensity. Conversely, cortical injection of the MEK inhibitor blocked nicotine's effect on the layer 2/3 sink (Fig. 4, *bottom*; paired *t*-tests, $P > 0.05$, $n = 6$ at each intensity) but not on the layer 4 sink ($P < 0.05$). The effects of nicotine and MEK inhibition, therefore, did not vary with acoustic intensity.

Thus blocking activation of MAPK in thalamus versus cortex differentially blocks nicotine-induced

J Neurophysiol
J Neurophysiol

enhancement of the initial layer 4 current sink versus the peak layer 2/3 current sink, indicating dependence on thalamocortical versus intracortical processes, respectively. Inhibition of MEK in either locus prevented enhancement of the peak layer 4 sink, suggesting underlying contributions from both thalamocortical and intracortical processes.

Nicotinic modulation of nonCF-evoked responses. Nicotine's effect on responses to non-CF stimuli (2 octaves below CF) differed consistently from its effect on CF-evoked responses at the same recording site (determined after a single nicotine injection, alternating CF and nonCF stimulus sets). Because the nonCF-evoked CSD profiles and the changes produced by nicotine were more varied than at CF (Kaur et al. 2005), we did not construct group CSD profiles but instead grouped data, using three different measures: *1*) peak current sink in layer 4, *2*) peak current sink in layer 2/3, and *3*) largest-amplitude sink, regardless of layer. As shown in Fig. 5*A* for an individual animal, even as nicotine enhanced responses to CF stimuli (Fig. 5*A*, *top*), at the same time it reduced responses to nonCF stimuli (Fig. 5*A*, *bottom*). In group data (Fig. 5*B*), nicotine reduced by ~20% the peak amplitude of the largest current sink evoked by nonCF stimuli (data combined from control animals after injection of U0124 into thalamus or cortex; paired *t*-test, $n = 12$, $P = 0.005$) and showed a tendency to reduce the peak sink in layer 4 ($P = 0.053$) but did not affect the peak sink in layer 2/3 ($P = 0.651$). Regardless of which measurement is employed, nicotine consistently increased the contrast between nonCF-evoked responses (either suppressed or not affected) and enhanced CF-evoked responses.

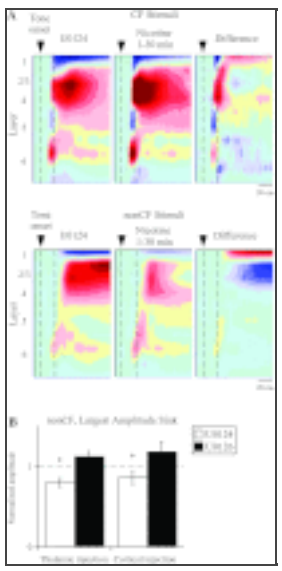

Fig. 5.

Effects of nicotine and MEK inhibition on CSD profiles evoked by spectrally distant (nonCF) stimuli. *A*: in this example, systemic nicotine simultaneously enhanced CF-evoked current sinks (*top*) and reduced most activity evoked in response to nonCF stimuli ...

To determine the contribution of MAPK activation to nicotinic suppression of nonCF-evoked responses, we measured the effects of MEK inhibitor on nicotinic regulation of the largest-amplitude current sink. After microinjection of U0126 into the thalamus or cortex, nicotine did not alter the amplitude of the largest current sink (Fig. 5*B*; thalamic injection, paired *t*-test, $n = 5$, $P = 0.199$; cortical injection, $n = 6$, $P = 0.217$). Thus the suppressive effect of nicotine on nonCF-evoked responses, as with its enhancing effect on CF-evoked responses, requires activation of MAPK.

Activated-MAPK immunofluorescence and dependence on cortical nAChRs. In a final set of experiments, we determined the distribution of cells in A1 with nicotine-induced activation of MAPK and the dependence on nAChRs that also are in A1 (as opposed to, for example, nAChRs regulating diffuse neurotransmitter systems originating in the brain stem that, in turn, project to A1). We subjected six adult mice to bilateral white noise acoustic stimulation and systemic nicotine after microinjecting auditory cortex in one hemisphere with control solution (ACSF) and in the contralateral hemisphere with a nAChR antagonist, either DHβE (50 nl, 1 μM) or MLA (10 nM) to block α4β2* or α7 nAChRs, respectively. In each animal, both intracortical injection sites were marked with fluorescent tracer (Fig. 6*A*). After 5 min of postnicotine acoustic stimulation, animals were perfused and the brains were

sectioned and processed for immunofluorescent labeling of phosphorylated MAPK (see MATERIALS AND METHODS).

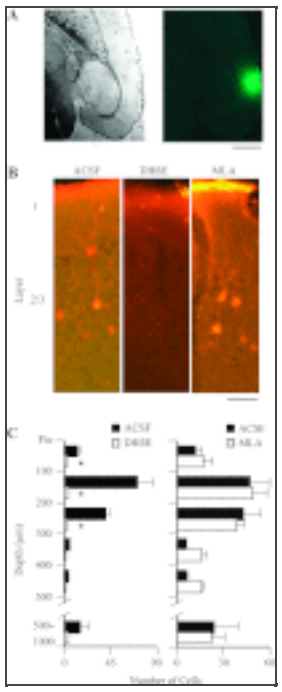

Fig. 6.

Distribution of cells with activated MAPK in A1 and dependence of activation on intracortical nicotinic acetylcholine receptors (nAChRs). *A*: horizontal tissue section with brightfield view (*left*) and fluorescence (*right*) showing location of drug injection **...**

In control hemispheres (ACSF microinjection), immunolabeled cells were found primarily in the upper layers of A1 (Fig. 6*B*), especially from 100 μm to 300 μm below the pia (Fig. 6*C*; ANOVAs comparing depth distributions in 100-μm bins, all $P < 0.05$). The majority of immunolabeled cells exhibited clear somatic staining but beyond that did not have readily identifiable morphology, and some cells exhibited short, vertically oriented processes (Fig. 6*B*). The immunolabeling of somata was blocked completely by intracortical DHβE but not affected by intracortical MLA (Fig. 6, *B* and *C*; ANOVAs comparing 100-μm-wide bins in control vs. drug hemispheres; DHβE: $P < 0.05$ for 0–100 μm, 100–200 μm, and 200–300 μm, $n = 3$ animals; MLA: $P > 0.05$ for all depths, $n = 3$ animals). Thus nicotinic activation of MAPK in A1 depends on α4β2*, but not α7, nAChRs that are also in A1.

In two additional animals, the brain was sectioned in a near-horizontal plane so as to preserve the thalamocortical pathway (Cruikshank et al. 2002). We focused on the first 1–2 mm of the thalamocortical pathway, including STR, looking for immunolabeled processes. Although STR and the portion of the thalamocortical pathway anterior to the hippocampus did contain diffuse, above-background levels of immunofluorescence, there were few identifiable processes and this approach was not pursued further.

DISCUSSION

Go to: Go to:

The results show that modulation of tone-evoked responses in A1 by systemic nicotine depends on MAPK-mediated signal transduction. Enhancement of CF-evoked current sinks in layers 4 and 2/3 involves independent activation of MAPK within thalamocortical and local intracortical circuits, whereas nicotinic suppression of responses to spectrally distant (nonCF) stimuli depends on MAPK to suppress activity along long-distance intracortical pathways. Activation of cortical MAPK in turn depends on activation of α4β2* nAChRs located in A1. Thus nicotinic modulation of spectral integration in A1, the end result of which is to shift cortical processing toward favoring CF stimuli, involves activation of MAPK in at least three distinct circuits.

Nicotinic "neuromodulation" via ionotropic nAChRs and MAPK. The nAChR is the prototypic ionotropic receptor, a ligand-gated ion channel best known for its role at the neuromuscular junction but also well known for actions in the brain (Albuquerque et al. 2009; Lester and Dani 1995; Pidoplichko et al. 1997). Neuronal nAChRs are pentamers comprised of α- and β-subunits, or only α-

subunits, that mediate multiple actions in cortex such as rapid postsynaptic excitation of interneurons and pyramidal neurons, presynaptic enhancement of neurotransmitter release, and, as shown recently, enhanced excitability of thalamocortical axons (Frazier et al. 1998; Gray et al. 1996; Grybko et al. 2011; Kawai et al. 2007; Roerig et al. 1997). Neuronal nAChRs gate a cation current of Na^+, K^+, and, depending on subunit composition, Ca^{2+} (Dajas-Bailador and Wonnacott 2004; Vernino et al. 1992). Rapid application of agonist demonstrates that nAChRs activate rapidly, and in the continued presence of agonist exhibit fast and slow components of desensitization, so that much of the current may subside within milliseconds (Pidoplichko et al. 1997; Zhang et al. 1994). In addition to Ca^{2+} influx via the receptor itself, nAChR activation can increase intracellular Ca^{2+} via voltage-gated Ca^{2+} channels or release from intracellular stores (Dajas-Bailador and Wonnacott 2004; Dickinson et al. 2008; Grybko et al. 2011; Sharma and Vijayaraghavan 2003); in principle, any of these Ca^{2+} sources could trigger biochemical signal transduction.

In contrast to the rapid ion fluxes gated by nAChRs, many studies at the systems and behavioral levels reveal more subtle effects of nicotine that endure for tens of minutes and contribute to perceptual and cognitive enhancement (see *Nicotinic activation of MAPK in sensory-cognitive function*). Potential mechanisms underlying nicotinic neuromodulation include sustained activation of a weakly desensitizing nAChR current by circulating nicotine (half-life in mouse ~9 min; Siu and Tyndale 2007) or activation of brain systems that exert conventional neuromodulatory actions via metabotropic receptors (see introduction). However, the present study indicates that neither of these potential mechanisms plays a major role in nicotine-induced neuromodulation of A1, since nicotinic effects were blocked by inhibition of MAPK activation (despite the continued presence of circulating nicotine) and MAPK activation was blocked by antagonism of cortical nAChRs (despite continued nicotinic stimulation of, for example, diffuse neurotransmitter systems originating in the brain stem or basal forebrain). Nicotinic activation of MAPK has been demonstrated in a variety of preparations, including cultured cortical neurons (Steiner et al. 2007), cortical synaptosomes (Dickinson et al. 2008), cell lines (Nakayama et al. 2001), and autonomic ganglia (Chang and Berg 2001). Systemic nicotine in vivo activates MAPK in frontal cortex, as demonstrated by immunolabeling and Western blot for phosphorylated ERK1/2 (Brunzell et al. 2003; Valjent et al. 2004). In most studies, however, the functional consequences of nicotine-induced MAPK activation on cortical circuits is not clear. The present study shows that activation of MAPK is required for nicotinic enhancement of sensory processing in A1.

MAPK-mediated regulation of distinct thalamocortical and intracortical circuits. Previous studies have shown that systemic nicotine enhances sensory-evoked cortical responses measured by recording single units, evoked potentials, and LFPs in humans, cats, rats, and mice (Harkrider and Champlin 2001; Kawai et al. 2011; Liang et al. 2006; Metherate 2004; Oldford and Castro-Alamancos 2003; Parkinson et al. 1988). The present study extends this observation to the critical involvement of MAPK and, importantly, implicates distinct loci of action. Although nAChRs are found throughout the auditory system (Morley and Happe 2000), the effects of systemic nicotine on processing in A1 clearly involve dependence on cortical nAChRs and modulation, via MAPK, of three functionally distinct forebrain circuits.

One locus of action lies along the auditory thalamocortical pathway that mediates the CF-evoked initial current sink in cortical layer 4. The onset and initial few milliseconds of the layer 4 current sink are affected by microinjection into the thalamus of nAChR antagonist (Kawai et al. 2007) or MEK inhibitor (present results) but not by intracortical injection of nAChR antagonist (Kawai et al. 2011),

MEK inhibitor (present study), or the GABA agonist muscimol (Happel et al. 2010; Kaur et al. 2004; Liu et al. 2007), indicating that this initial portion of the layer 4 current sink reflects monosynaptic thalamocortical input. Nicotinic enhancement of thalamocortical input likely involves enhanced excitability of myelinated thalamocortical axons (Kawai et al. 2007), which relay information about CF stimuli to A1. The initial segment of the thalamocortical pathway was the target of microinjections in the present study, but since injections likely spread beyond this narrow pathway other thalamic structures may be implicated. Similarly, the subcortical white matter though which the myelinated thalamocortical pathway projects also exhibits binding for nAChRs (Bieszczad et al. 2012) and may have been affected by microinjections in the present study. Regardless of the exact locus, the results clearly show that nicotinic enhancement of cortical responsiveness involves enhanced thalamocortical input.

A second locus of action is intracortical and also contributes to enhanced responses to CF stimuli. Thalamocortical input to layer 4 of A1, as in other sensory cortices (Douglas and Martin 2004), is rapidly amplified by local circuits to produce a large current sink in layer 2/3 (Happel et al. 2010; Kaur et al. 2005; Kawai et al. 2011; Liu et al. 2007). In the present study, nicotinic enhancement of this layer 2/3 sink was blocked by cortical, but not thalamic, injections of MEK inhibitor, and immunolabel for activated MAPK in layer 2/3 was blocked by intracortical DHβE. These results complement the recent physiological demonstration that intracortical DHβE blocks nicotinic enhancement of the layer 2/3 current sink (Kawai et al. 2011). Together, these results indicate a local nicotinic action within A1, one that involves cortical α4β2* nAChRs and subsequent activation of MAPK. Importantly, these results also indicate that nicotinic enhancement of intracortical responses occurs independently of enhanced thalamocortical input. Moreover, since endogenous cholinergic systems innervate thalamus and cortex separately, i.e., from cholinergic nuclei in the brain stem versus basal forebrain, respectively (Everitt and Robbins 1997), our findings imply that activation of thalamic versus cortical MAPK could occur independently.

The third locus of action lies along long-distance ("horizontal") intracortical pathways that mediate responses to spectrally distant, nonCF stimuli. Previous studies have employed a variety of methods, notably CSD analysis and intracortical silencing via muscimol administration, to demonstrate that cortical responses to spectrally distant stimuli depend on long-distance intracortical projections from regions of A1 where the stimulus is CF (Happel et al. 2010; Kaur et al. 2004, 2005). The present results showing differential effects of nicotine on CF- versus nonCF-evoked responses—e.g., enhancement versus either suppression or no effect, respectively—further support the notion of distinct underlying circuits (see also similar findings from Kawai et al. 2011). Blockade of nicotinic suppression by MEK inhibition implies regulation of long-distance pathways. The apparent activation of layer 1 by nicotine in some cases (e.g., Fig. 5*A*, nonCF "Difference" profile) suggests a role for layer 1 interneurons that are excited by nicotine and in turn inhibit layers 2/3 (Christophe et al. 2002; Lee et al. 2010) and may regulate long-distance projections mediating nonCF responses (Metherate 2011a). Note that an unresolved issue relates to the physical arrangement of nAChRs and MAPK within auditory cortex. For example, it is not known whether nAChRs and MAPK are colocalized in the same neuron. Methods for visualizing nAChRs and MAPK will be useful for resolving this issue.

Nicotinic activation of MAPK in sensory-cognitive function. The present results also could help elucidate the role of nAChRs in cognitive function, given an extensive literature implicating MAPK as a critical node among signaling pathways mediating behaviorally relevant synaptic plasticity (Philips et al. 2007; Reissner et al. 2006; Sweatt 2004; Waltereit et al. 2001; Welsby et al. 2009). Experience-

dependent plasticity in sensory cortex is thought to require a convergence of sensory inputs with inputs mediating the effects of behavioral attention (Carpenter-Hyland et al. 2010; Fritz et al. 2003; Weinberger 2004). Since nAChRs contribute to attentional mechanisms (Hasselmo and Sarter 2011), an attractive notion is that MAPK may serve as a molecular "node" (Reissner et al. 2006) or coincidence detector (Sweatt 2001) to signal concurrent sensory stimulation and attention. Such interactions may occur along multiple timescales (Philips et al. 2007; Shobe et al. 2009): In the short term, nicotinic "sharpening" of receptive fields (enhancement of CF-evoked responses, suppression of nonCF-evoked responses) may contribute to mechanisms of "attentional narrowing" or filtering (Kassel 1997; Metherate 2011a). Over a longer term, nicotinic activation of MAPK may contribute to learning-related synaptic plasticity (London and Clayton 2008; Sweatt 2004; Welsby et al. 2009). These issues will be the focus of future investigations.

GRANTS

Go to: Go to:

This research was supported by National Institute of Drug Abuse Grant R01 DA-12929 and National Institute on Deafness and Other Communications Disorders Grants R01 DC-02967 and P30 DC-08369.

DISCLOSURES

Go to: Go to:

No conflicts of interest, financial or otherwise, are declared by the author(s).

AUTHOR CONTRIBUTIONS

Go to: Go to:

Author contributions: I.I. and R.M. conception and design of research; I.I. performed experiments; I.I. and R.M. analyzed data; I.I. and R.M. interpreted results of experiments; I.I. and R.M. prepared figures; I.I. and R.M. drafted manuscript; I.I. and R.M. edited and revised manuscript; I.I. and R.M. approved final version of manuscript.

ACKNOWLEDGMENTS

Go to: Go to:

We thank Ronit Lazar and Dr. Candace Hsieh for assistance with immunofluorescence experiments and Drs. Thomas J. Carew and Gary Phillips for helpful discussions about MAPK.

REFERENCES

Go to: Go to:

Abdala-Valencia et al., 2011. Abdala-Valencia H, Berdnikovs S, Cook-Mills JM. Mechanisms for vascular cell adhesion molecule-1 activation of ERK1/2 during leukocyte transendothelial migration. PloS One 6: e26706, 2011 [PMC free article] [PubMed]

Albuquerque et al., 2009. Albuquerque EX, Pereira EF, Alkondon M, Rogers SW. Mammalian nicotinic acetylcholine receptors: from structure to function. Physiol Rev 89: 73–120, 2009 [PMC free article] [PubMed]

Anderson et al., 2009. Anderson LA, Christianson GB, Linden JF. Mouse auditory cortex differs from visual and somatosensory cortices in the laminar distribution of cytochrome oxidase and acetylcholinesterase. Brain Res 1252: 130–142, 2009 [PubMed]

Azam et al., 2003. Azam L, Winzer-Serhan U, Leslie FM. Co-expression of alpha7 and beta2 nicotinic acetylcholine receptor subunit mRNAs within rat brain cholinergic neurons. Neuroscience 119: 965–977, 2003 [PubMed]

Bieszczad et al., 2012. Bieszczad KM, Kant R, Constantinescu CC, Pandey SK, Kawai HD, Metherate R, Weinberger NM, Mukherjee J. Nicotinic acetylcholine receptors in rat forebrain that bind ^{18}F-nifene: relating PET imaging, autoradiography and behavior. Synapse 66: 418–434, 2012 [PMC free article] [PubMed]

Brunzell et al., 2003. Brunzell DH, Russell DS, Picciotto MR. In vivo nicotine treatment regulates mesocorticolimbic CREB and ERK signaling in C57Bl/6J mice. J Neurochem 84: 1431–1441, 2003 [PubMed]

Carpenter-Hyland et al., 2010. Carpenter-Hyland EP, Plummer TK, Vazdarjanova A, Blake DT. Arc expression and neuroplasticity in primary auditory cortex during initial learning are inversely related to neural activity. Proc Natl Acad Sci USA 107: 14828–14832, 2010 [PMC free article] [PubMed]

Chang and Berg, 2001. Chang KT, Berg DK. Voltage-gated channels block nicotinic regulation of CREB phosphorylation and gene expression in neurons. Neuron 32: 855–865, 2001 [PubMed]

Christophe et al., 2002. Christophe E, Roebuck A, Staiger JF, Lavery DJ, Charpak S, Audinat E. Two types of nicotinic receptors mediate an excitation of neocortical layer I interneurons. J Neurophysiol 88: 1318–1327, 2002 [PubMed]

Cruikshank et al., 2002. Cruikshank SJ, Rose HJ, Metherate R. Auditory thalamocortical synaptic transmission in vitro. J Neurophysiol 87: 361–384, 2002 [PubMed]

Dajas-Bailador and Wonnacott, 2004. Dajas-Bailador F, Wonnacott S. Nicotinic acetylcholine receptors and the regulation of neuronal signalling. Trends Pharmacol Sci 25: 317–324, 2004 [PubMed]

Dickinson et al., 2008. Dickinson JA, Kew JN, Wonnacott S. Presynaptic alpha7- and beta2-containing nicotinic acetylcholine receptors modulate excitatory amino acid release from rat prefrontal cortex nerve terminals via distinct cellular mechanisms. Mol Pharmacol 74: 348–359, 2008 [PubMed]

Douglas and Martin, 2004. Douglas RJ, Martin KA. Neuronal circuits of the neocortex. Annu Rev Neurosci 27: 419–451, 2004 [PubMed]

Everitt and Robbins, 1997. Everitt BJ, Robbins TW. Central cholinergic systems and cognition. Annu Rev Psychol 48: 649–684, 1997 [PubMed]

Faber et al., 2011. Faber A, Corcoran RB, Ebi H, Sequist LV, Waltman BA, Chung E, Incio J, Digumarthy SR, Pollack SF, Song Y, Muzikansky A, Lifshits E, Roberge S, Coffman EJ, Benes C, Gomez H, Baselga J, Arteaga CL, Rivera MN, Dias-Santagata D, Jain RK, Engelman JA. BIM expression in treatment naive cancers predicts responsiveness to kinase inhibitors. Cancer Discov 1: 352–365, 2011 [PMC free article] [PubMed]

Favata et al., 1998. Favata MF, Horiuchi KY, Manos EJ, Daulerio AJ, Stradley DA, Feeser WS, Van Dyk DE, Pitts WJ, Earl RA, Hobbs F, Copeland RA, Magolda RL, Scherle PA, Trzaskos JM. Identification of a novel inhibitor of mitogen-activated protein kinase kinase. J Biol Chem 273: 18623–18632, 1998 [PubMed]

Frazier et al., 1998. Frazier CJ, Buhler AV, Weiner JL, Dunwiddie TV. Synaptic potentials mediated via alpha-bungarotoxin-sensitive nicotinic acetylcholine receptors in rat hippocampal interneurons. J Neurosci 18: 8228–8235, 1998 [PubMed]

Fritz et al., 2003. Fritz J, Shamma S, Elhilali M, Klein D. Rapid task-related plasticity of

spectrotemporal receptive fields in primary auditory cortex. Nat Neurosci 6: 1216–1223, 2003 [PubMed]

Gray et al., 1996. Gray R, Rajan AS, Radcliffe KA, Yakehiro M, Dani JA. Hippocampal synaptic transmission enhanced by low concentrations of nicotine. Nature 383: 713–716, 1996 [PubMed]

Grybko et al., 2011. Grybko MJ, Hahm ET, Perrine W, Parnes JA, Chick WS, Sharma G, Finger TE, Vijayaraghavan S. A transgenic mouse model reveals fast nicotinic transmission in hippocampal pyramidal neurons. Eur J Neurosci 33: 1786–1798, 2011 [PMC free article] [PubMed]

Happel et al., 2010. Happel MF, Jeschke M, Ohl FW. Spectral integration in primary auditory cortex attributable to temporally precise convergence of thalamocortical and intracortical input. J Neurosci 30: 11114–11127, 2010 [PubMed]

Harkrider and Champlin, 2001. Harkrider AW, Champlin CA. Acute effect of nicotine on non-smokers. III. LLRs and EEGs. Hear Res 160: 99–110, 2001 [PubMed]

Hasselmo and Sarter, 2011. Hasselmo ME, Sarter M. Modes and models of forebrain cholinergic neuromodulation of cognition. Neuropsychopharmacology 36: 52–73, 2011 [PMC free article] [PubMed]

Kassel, 1997. Kassel JD. Smoking and attention: a review and reformulation of the stimulus-filter hypothesis. Clin Psychol Rev 17: 451–478, 1997 [PubMed]

Kaur et al., 2004. Kaur S, Lazar R, Metherate R. Intracortical pathways determine breadth of subthreshold frequency receptive fields in primary auditory cortex. J Neurophysiol 91: 2551–2567, 2004 [PubMed]

Kaur et al., 2005. Kaur S, Rose HJ, Lazar R, Liang K, Metherate R. Spectral integration in primary auditory cortex: laminar processing of afferent input, in vivo and in vitro. Neuroscience 134: 1033–1045, 2005 [PubMed]

Kawai et al., 2007. Kawai H, Lazar R, Metherate R. Nicotinic control of axon excitability regulates thalamocortical transmission. Nat Neurosci 10: 1168–1175, 2007 [PubMed]

Kawai et al., 2011. Kawai HD, Kang HA, Metherate R. Heightened nicotinic regulation of auditory cortex during adolescence. J Neurosci 31: 14367–14377, 2011 [PMC free article] [PubMed]

Lee et al., 2010. Lee S, Hjerling-Leffler J, Zagha E, Fishell G, Rudy B. The largest group of superficial neocortical GABAergic interneurons expresses ionotropic serotonin receptors. J Neurosci 30: 16796–16808, 2010 [PMC free article] [PubMed]

Lester and Dani, 1995. Lester RA, Dani JA. Acetylcholine receptor desensitization induced by nicotine in rat medial habenula neurons. J Neurophysiol 74: 195–206, 1995 [PubMed]

Levin et al., 2006. Levin ED, McClernon FJ, Rezvani AH. Nicotinic effects on cognitive function: behavioral characterization, pharmacological specification, and anatomic localization. Psychopharmacology (Berl) 184: 523–539, 2006 [PubMed]

Liang et al., 2006. Liang K, Poytress BS, Chen Y, Leslie FM, Weinberger NM, Metherate R. Neonatal nicotine exposure impairs nicotinic enhancement of central auditory processing and auditory learning in adult rats. Eur J Neurosci 24: 857–866, 2006 [PubMed]

J Neurophysiol
J Neurophysiol

Liang et al., 2008. Liang K, Poytress BS, Weinberger NM, Metherate R. Nicotinic modulation of tone-evoked responses in auditory cortex reflects the strength of prior auditory learning. Neurobiol Learn Mem 90: 138–146, 2008 [PMC free article] [PubMed]

Liu et al., 2007. Liu BH, Wu GK, Arbuckle R, Tao HW, Zhang LI. Defining cortical frequency tuning with recurrent excitatory circuitry. Nat Neurosci 10: 1594–1600, 2007 [PMC free article] [PubMed]

London and Clayton, 2008. London SE, Clayton DF. Functional identification of sensory mechanisms required for developmental song learning. Nat Neurosci 11: 579–586, 2008 [PMC free article] [PubMed]

Metherate, 2011a. Metherate R. Functional connectivity and cholinergic modulation in auditory cortex. Neurosci Biobehav Rev 35: 2058–2063, 2011a [PMC free article] [PubMed]

Metherate, 2011b. Metherate R. Modulatory mechanisms for controlling auditory processing. In: Synaptic Mechanisms in the Auditory System, edited by Trussell LO, Popper AN, Fay RR, editors. New York: Springer, 2011b, p. 187–202

Metherate, 2004. Metherate R. Nicotinic acetylcholine receptors in sensory cortex. Learn Mem 11: 50–59, 2004 [PubMed]

Miyazawa et al., 2003. Miyazawa A, Fujiyoshi Y, Unwin N. Structure and gating mechanism of the acetylcholine receptor pore. Nature 423: 949–955, 2003 [PubMed]

Morley and Happe, 2000. Morley BJ, Happe HK. Cholinergic receptors: dual roles in transduction and plasticity. Hear Res 147: 104–112, 2000 [PubMed]

Muller-Preuss and Mitzdorf, 1984. Muller-Preuss P, Mitzdorf U. Functional anatomy of the inferior colliculus and the auditory cortex: current source density analyses of click-evoked potentials. Hear Res 16: 133–142, 1984 [PubMed]

Nakayama et al., 2001. Nakayama H, Numakawa T, Ikeuchi T, Hatanaka H. Nicotine-induced phosphorylation of extracellular signal-regulated protein kinase and CREB in PC12h cells. J Neurochem 79: 489–498, 2001 [PubMed]

Oldford and Castro-Alamancos, 2003. Oldford E, Castro-Alamancos MA. Input-specific effects of acetylcholine on sensory and intracortical evoked responses in the “barrel cortex” in vivo. Neuroscience 117: 769–778, 2003 [PubMed]

Parkinson et al., 1988. Parkinson D, Kratz KE, Daw NW. Evidence for a nicotinic component to the actions of acetylcholine in cat visual cortex. Exp Brain Res 73: 553–568, 1988 [PubMed]

Philips et al., 2007. Philips GT, Tzvetkova EI, Carew TJ. Transient mitogen-activated protein kinase activation is confined to a narrow temporal window required for the induction of two-trial long-term memory in *Aplysia*. J Neurosci 27: 13701–13705, 2007 [PubMed]

Picciotto et al., 2008. Picciotto MR, Addy NA, Mineur YS, Brunzell DH. It is not “either/or”: activation and desensitization of nicotinic acetylcholine receptors both contribute to behaviors related to nicotine addiction and mood. Prog Neurobiol 84: 329–342, 2008 [PMC free article] [PubMed]

Pidoplichko et al., 1997. Pidoplichko VI, DeBiasi M, Williams JT, Dani JA. Nicotine activates and desensitizes midbrain dopamine neurons. Nature 390: 401–404, 1997 [PubMed]

Reissner et al., 2006. Reissner KJ, Shobe JL, Carew TJ. Molecular nodes in memory processing: insights from *Aplysia*. Cell Mol Life Sci 63: 963–974, 2006 [PubMed]

Roberson et al., 1999. Roberson ED, English JD, Adams JP, Selcher JC, Kondratick C, Sweatt JD. The mitogen-activated protein kinase cascade couples PKA and PKC to cAMP response element binding protein phosphorylation in area CA1 of hippocampus. J Neurosci 19: 4337–4348, 1999 [PubMed]

Roerig et al., 1997. Roerig B, Nelson DA, Katz LC. Fast synaptic signaling by nicotinic acetylcholine and serotonin 5-HT_3 receptors in developing visual cortex. J Neurosci 17: 8353–8362, 1997 [PubMed]

Sharma and Vijayaraghavan, 2003. Sharma G, Vijayaraghavan S. Modulation of presynaptic store calcium induces release of glutamate and postsynaptic firing. Neuron 38: 929–939, 2003 [PubMed]

Shobe et al., 2009. Shobe JL, Zhao Y, Stough S, Ye X, Hsuan V, Martin KC, Carew TJ. Temporal phases of activity-dependent plasticity and memory are mediated by compartmentalized routing of MAPK signaling in *Aplysia* sensory neurons. Neuron 61: 113–125, 2009 [PMC free article] [PubMed]

Siu and Tyndale, 2007. Siu EC, Tyndale RF. Characterization and comparison of nicotine and cotinine metabolism in vitro and in vivo in DBA/2 and C57BL/6 mice. Mol Pharmacol 71: 826–834, 2007 [PubMed]

Song et al., 2008. Song P, Sekhon HS, Fu XW, Maier M, Jia Y, Duan J, Proskosil BJ, Gravett C, Lindstrom J, Mark GP, Saha S, Spindel ER. Activated cholinergic signaling provides a target in squamous cell lung carcinoma. Cancer Res 68: 4693–4700, 2008 [PMC free article] [PubMed]

Steiner et al., 2007. Steiner RC, Heath CJ, Picciotto MR. Nicotine-induced phosphorylation of ERK in mouse primary cortical neurons: evidence for involvement of glutamatergic signaling and CaMKII. J Neurochem 103: 666–678, 2007 [PubMed]

Stiebler et al., 1997. Stiebler I, Neulist R, Fichtel I, Ehret G. The auditory cortex of the house mouse: left-right differences, tonotopic organization and quantitative analysis of frequency representation. J Comp Physiol A 181: 559–571, 1997 [PubMed]

Sweatt, 2004. Sweatt JD. Mitogen-activated protein kinases in synaptic plasticity and memory. Curr Opin Neurobiol 14: 311–317, 2004 [PubMed]

Sweatt, 2001. Sweatt JD. The neuronal MAP kinase cascade: a biochemical signal integration system subserving synaptic plasticity and memory. J Neurochem 76: 1–10, 2001 [PubMed]

Valjent et al., 2004. Valjent E, Pages C, Herve D, Girault JA, Caboche J. Addictive and non-addictive drugs induce distinct and specific patterns of ERK activation in mouse brain. Eur J Neurosci 19: 1826–1836, 2004 [PubMed]

Vernino et al., 1992. Vernino S, Amador M, Luetje CW, Patrick J, Dani JA. Calcium modulation and high calcium permeability of neuronal nicotinic acetylcholine receptors. Neuron 8: 127–134, 1992 [PubMed]

Waltereit et al., 2001. Waltereit R, Dammermann B, Wulff P, Scafidi J, Staubli U, Kauselmann G, Bundman M, Kuhl D. Arg3.1/Arc mRNA induction by Ca^{2+} and cAMP requires protein kinase A and mitogen-activated protein kinase/extracellular regulated kinase activation. J Neurosci 21: 5484–5493, 2001 [PubMed]

Weinberger, 2004. Weinberger NM. Specific long-term memory traces in primary auditory cortex. Nat

Rev Neurosci 5: 279–290, 2004 [PMC free article] [PubMed]

Welsby et al., 2009. Welsby PJ, Rowan MJ, Anwyl R. Intracellular mechanisms underlying the nicotinic enhancement of LTP in the rat dentate gyrus. Eur J Neurosci 29: 65–75, 2009 [PubMed]

Zhang et al., 1994. Zhang ZW, Vijayaraghavan S, Berg DK. Neuronal acetylcholine receptors that bind alpha-bungarotoxin with high affinity function as ligand-gated ion channels. Neuron 12: 167–177, 1994 [PubMed]